Local site effect microzonation of Lorca town (SE Spain)

**M. Navarro · A. García-Jerez · F. J. Alcalá ·
F. Vidal · T. Enomoto**

Abstract Local site effect assessment based on subsurface ground conditions is often the
key to evaluate urban seismic hazard. The site effect evaluation in Lorca town (south-eastern
Spain) started with a classification of urban geology through the geological mapping at scale
1:10,000 and the use of geotechnical data and geophysical surveys. The 17 geological for-
mations identified were classified into 5 geological/seismic formations according to their
seismic amplification capacity obtained from ambient vibration measurements as well as
from simultaneous strong motion records. The shear-wave velocity structure of each geo-
logical/seismic formation was evaluated by means of inversion of Rayleigh wave dispersion
data obtained from vertical-component array records of ambient noise. Nakamura's method
was applied to determine a predominant period distribution map. The spectral amplification
factors were fourfold the values recorded in a reference hard-rock site. Finally, the capability
of this study for explaining the damage distribution caused by the May 11th, 2011 Lorca
destructive earthquake (Mw = 5.2) was examined. The methods used in this work are of

M. Navarro (✉) · A. García-Jerez
Dept. de Química y Física, University of Almería, 04120 Almeria, Spain
e-mail: mnavarro@ual.es

A. García-Jerez
e-mail: agj574@ual.es

M. Navarro · A. García-Jerez · F. Vidal
Instituto Andaluz de Geofísica, University of Granada, 18070 Granada, Spain
e-mail: fvidal@iag.iag.ugr.es

F. J. Alcalá
Geo-Systems Centre (CVRM-IST), Technical University of Lisbon, 1049-001 Lisbon, Portugal
e-mail: francisco.alcala@ist.utl.pt

F. Vidal
Dept. de Física Teórica y del Cosmos, University of Granada, Granada, Spain

T. Enomoto
Department of Building Engineering, University of Kanagawa, Yokohama, Japan
e-mail: enomot01@kanaga-u.ac.jp

assistance to evaluate ground amplification phenomena in urban areas of complex geology as Lorca town due to future earthquakes with applicability on urban seismic risk management.

Keywords   Landform classification · Ambient noise · SPAC method · Shallow S-wave velocity structure · Predominant period · Strong motion · Lorca earthquake

1 Introduction

Lorca town, with 91,000 inhabitants and 3.5 km × 1.5 km urban area surface, is located in Murcia province (south-eastern Spain). This area belongs to the eastern part of the Betic region, an Alpine chain placed at the western most part of the Eurasian and African Plates interaction zone (Alcalá et al. 2013). In spite of the low moderate seismic activity of this region in a worldwide context, this is the most hazardous seismic area of Spain. As shown in the probabilistic seismic hazard map of the Spanish Building Code (NCSE-02 2002), in south-eastern Spain there are extensive areas where peak ground acceleration (PGA) on rock are greater than 0.12 g for a 475-year return period, even reaching 0.25 g in some zones. According to NCSE-02, Lorca town and most of the Murcia province have a relatively significant seismic hazard (PGA $\geq$ 0.12 g).

The Betic region is characterized by frequent earthquakes of small and moderate magnitude with moment magnitude (Mw) generally smaller than 5.5. However, most of the largest and destructive historical earthquakes occurred during the last six centuries in Spain took place in this region (Vidal 1986). Among them, there were some with epicentral macroseismic intensity $I_0 \geq$ VIII (EMS-98 scale) (European Macroseismic Scale 1998), as those of 1518 (Vera), 1522 (Almeria), 1531 (Baza), 1658 (Almeria), 1674 (Lorca), 1804 (Adra), and 1829 (Torrevieja), all of them with epicentral distances (Δ) to Lorca town smaller than 150 km (Vidal 1986).

Other historical damaging events ($I_0 \sim$ VII) affected Lorca with $\Delta < 50$ km; e.g. the 1579 and 1818 ones with epicentres close to the town, and the 1855 and 1907 earthquakes placed nearby Alhama de Murcia and Totana towns, respectively. All these damaging earthquakes are located along the strike-slip Alhama de Murcia Fault System, which has been active during the Late Miocene and the Quaternary (Bousquet 1979; Alfaro et al. 2002; Martínez Díaz and Hernández-Enrile 2001; Masana et al. 2004; García-Mayordomo 2005).

Three additional shocks have occurred in 1999 (Mula), 2002 (Bullas), and 2005 (La Paca) near Lorca town with magnitudes (Mw) of 4.7, 5.0, and 4.8, respectively, and I_0 ranging from VI to VII (EMS-98 scale) (Benito et al. 2006). These events have shown the relevance of shallow geology for explanation of both the ground motion amplification, and the degree and spatial distribution of building destruction (Navarro et al. 2000; Benito et al. 2006). During the course of this research, two new shallow earthquakes occurred on May 11th, 2011 with epicentre in Lorca town (Mw = 4.6 and 5.2 and maximum macroseismic intensity (Imax) = VI and VII, respectively), highlighting again the relevance of the features of the earthquake ground response and its influence on building behaviour during the shaking.

The influence of shallow geology and topography on the local amplification of the shaking is named the site effect. Far from steep slopes as well as for wide ranges of wavelengths, topographic effects are negligible (e.g. Ashford et al. 1997). The relevance of site effects in the earthquake ground motion features affecting the degree of damage to man-made structures in urban areas (Bakir et al. 2002; Navarro et al. 2004; Mucciarelli et al. 2002) was described

for large earthquakes [e.g. Colima, Mexico, 2003 (Navarro et al. 2008); N Pakistan, 2005 (Maqsood and Schwarz 2008); Sichuan, China, 2008 (Peng Cui et al. 2011); Maule, Chile, 2010 (Aranda et al. 2012)] as well as for moderate events [e.g. Izmit, Turkey, 1999 (Barka 1999); Algeria, 2003 (Laouamia et al. 2006); Al Hoceima, Morocco, 2004 (Vidal et al. 2004); L'Aquila, Italy, 2009 (Cucci and Tertulliani 2011)], and small ones [e.g. Molisse, Italy, 2002 (Mucciarelli et al. 2002); Adra, Spain, 1993 (Navarro et al. 2007); and the abovementioned events in south-eastern Spain]. A good correlation is often found between local site amplification and the type, thickness, and age of unconsolidated geological formations (Lachet et al. 1996). These facts have been also supported by many theoretical studies (e.g. Olsen et al. 1995; Alguacil et al. 2013).

Site effect sometimes explains ground motion amplifications found in narrow high-frequency bands which may have severe effects on the degree and spatial distribution of building destruction, as reported by Navarro et al. (2008) in Villa de Alvarez town (Mexico) due to the 2003 Colima earthquake. Variation in the ground behaviour was clearly observed attending to the ambient noise H/V spectral ratio at damaged and undamaged zones. Clear spectral peaks were found in a short period range between 0.1 and 0.2 s in the heavily damaged zone, whereas these peaks did not appear at the undamaged ones (Navarro et al. 2008).

The December 23rd, 1993 and the January 4th, 1994 Adra earthquakes are examples of amplification due to site effects in small events. The most relevant damage in Adra town occurred in reinforced concrete (RC) buildings from four to five storeys placed on $\sim$ 30 m thick alluvial sediments with a ground predominant period of around 0.2 s (Navarro et al. 2007). The influence of resonance phenomena is also suspected in the case of the February 2nd, 1999 Mula earthquake (García-Jerez et al. 2008). RC structures with four and five stories located in the central and western parts of Mula town over alluvial sediments had the more serious damage than those located in northern part of the town over bedrocks. Thus, site effects caused by the shallow ground structure (García-Jerez et al. 2008) and resonance phenomena between shallow geology and building probably had strong influence on the RC buildings damage distribution.

The stiffness degree and thickness of geological materials are two key properties that modulate the strength of the earthquake shaking. Since the National Earthquake Hazards Reduction Program (NEHRP 2003) soil classification in 1994, the mean shear-wave velocity in the uppermost 30 m ground thickness (V_S^{30}) has been adopted as a representative site characteristic parameter in several official seismic codes (e.g. NCSE-02; Eurocode-8 (EC8)) for building code implementations (e.g. Dobry et al. 2000), as well as in regional soil classification for seismic site effect evaluation (Alcalá et al. 2002; Ismet et al. 2006; Benito et al. 2010).

In order to determine the seismic behaviour of shallow geological structures, the relation between surface wave dispersion curves and elastic properties of the ground has been widely used in geophysical prospecting, using earthquakes or controlled sources for derivation of 1-D layered ground models (e.g. Nazarian 1984; Navarro et al. 1997; Tokimatsu 1997; Park et al. 1999). Along these lines, the capability of the spatial autocorrelation method (SPAC method; Aki 1957) and its related techniques of ambient noise analysis (e.g., García-Jerez et al. 2008; Garcia-Jerez et al. 2010) have been proved as innovative and convenient ways for determining the elastic properties of shallow sedimentary deposits in this kind of studies (e.g., Parolai et al. 2005; García-Jerez et al. 2007a).

This paper deals with the local site effect evaluation in Lorca town to explain the damage distribution caused by the Lorca 2011 destructive earthquake. For this objective of large interest in seismic risk management, the seismic behaviour of each geological formation

identified was characterized in terms of the average shear-wave velocity deduced from array records of ambient noise by applying the SPAC method and complementary shear-wave velocity data. A seismic microzonation in terms of predominant periods of shallow geology was subsequently obtained, as well as the ground seismic amplification from simultaneous strong motion records at different ground conditions by using the reference site method.

2 Geological setting

2.1 Regional geology and tectonic framework

Lorca town belongs to the eastern part of the Alpine Betic Chain, in southeast Spain (Fig. 1), which includes two main domains: the Internal and the External Betic Zones. The Internal Zone includes three tectonic complexes: the Nevado-Filabride Complex, which does not outcrop in the vicinity of Lorca town; the Alpujarride Complex, which overlies the Nevado-Filabride Complex and consists of low to medium grade metamorphic rocks; and the upper and mainly unmetamorphosed Malaguide Complex (Paquet 1969; Sanz de Galdeano et al. 1995). The External Zone represents the passive margin of the Iberian Plate which does not outcrop in the vicinity of Lorca (García-Hernández et al. 1980).

The convergence between the African and Eurasian Plates has produced a regional NNW-SSE tectonic compression from the Tertiary. A great displacement of crustal and sub-crustal (Internal Zone) took place ending with the collision of the Internal and External Betic Zones during the middle Burdigalian (Zeck et al. 1989; Alcalá et al. 2013). The inversion and deformation of the passive margin (External Zone) have taken place producing sinistral strike-slip motion regional faults with an ENE-WSW direction, which appears to control the structure of the ranges and the sedimentation rates of the basins in Southern Spain (Sanz de Galdeano et al. 1995). In the immediacy of Lorca town, the Guadalentín River is one of these basins contoured by the strike-slip Alhama de Murcia Fault System northward (Paquet 1969; Egeler et al. 1981; Silva et al. 1992). This system can be divided in two segments neighbouring Lorca town according to a different seismic behaviour: Lorca-Totana and Puerto Lumbreras-Lorca, with 23 and 28 km surface length and 0.30 and 0.41 meters per kiloyear of slip rate, respectively (García-Mayordomo 2005). The maximum moment magnitude estimated on each of these segments is 6.7 and 6.8 and the mean recurrence period (MRP) of such maximum events range between 2,000–5,000 years and 7,000–10,000 years, respectively (García-Mayordomo and Álvarez-Gómez 2006; García-Mayordomo and Martínez-Díaz 2006). The neotectonic activity controls the Quaternary geomorphologic evolution of the sedimentary record according to the main tectonic pulses.

2.2 Urban geology of Lorca town

The identification and classification of urban geology of Lorca town was a step to perform a geological mapping at scale 1:10,000 (Fig. 1) and to interpret the spatial geometry of geological formations. Data on field geology: 14 field-ground testing data, mechanical and geotechnical data from geotechnical reports: 40 mechanical drillings, and geophysics surveys from IGME (1992): 27 electrical geophysical tests and 10 shallow refraction profiles with 10-50-m-average penetrating thickness (Fig. 2), were the supporting data used for the mechanical and physical characterization of geological materials (Table 1).

Five main geological/seismic formations were clustered in Lorca town by combining the geological, geotechnical, and geophysical information of each 17 geological formations

BEEE720_rev
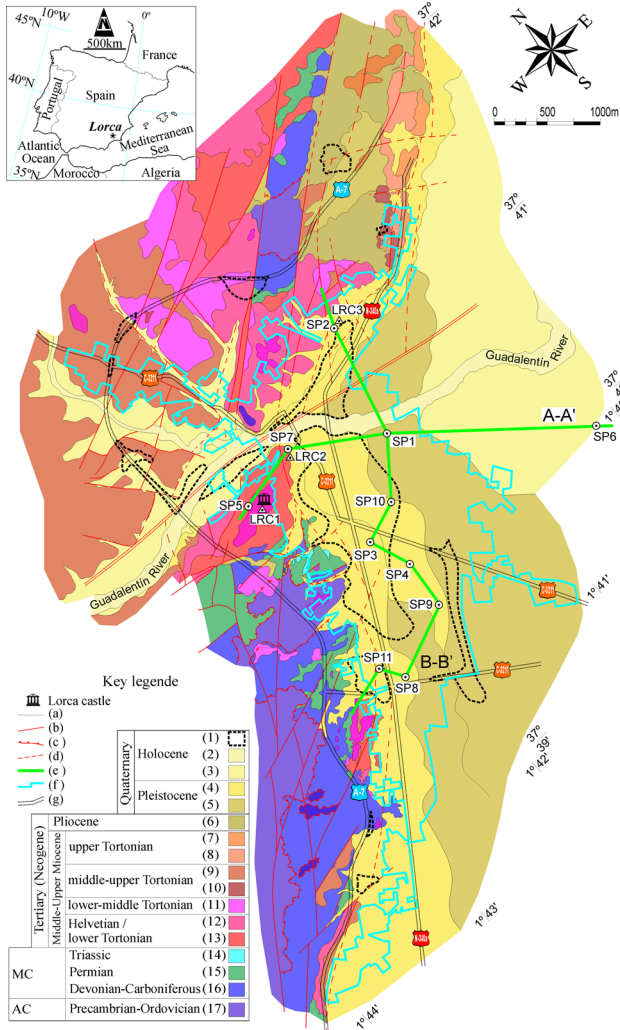
Fig. 1 Geological mapping of Lorca town at scale 1:10,000. Geological formations: *1* Cropland and anthropogenic fillings, *2* Alluvial terraces, *3* Colluvials, *4* Glacis III, *5* Glacis II, *6* Glacis I, *7* Sandy marls and breccias, *8* Gypsum and marls, *9* Marls, *10* Breccias and marls, *11* Conglomerates, sandstone and marls, *12* Marls, gypsum and sandstone, *13* Polygenic conglomerates, *14* Dolomitic limestone, *15 Red* clays, slates and quartzite, *16* Phyllite, schist and quartzite, *17* Schist, phyllite, and quartzite; MC Malaguide Complex; AC Alpujarride Complex; (*a*) undifferentiated geological contact; (*b*) normal fault; (*c*) thrust fault; (*d*) inferred fault; (e) geological/seismic cross-sections *A-A′* and *B-B′* singled out in Fig. 11; (*f*) urban boundary; (*g*) main roads. Array and accelerometers locations have been labelled from *SP1* to *SP11* and from *LRC1* to *LRC3*, respectively

identified (Fig. 1; Table 1): (1) Palaeozoic to Triassic pre-orogenic metamorphic hard-rock (bedrock), which includes schist, phyllite, quartzite, and dolomitic limestone from the Alpujarride and Malaguide Complexes; (2) Middle-Upper Miocene post-orogenic medium-
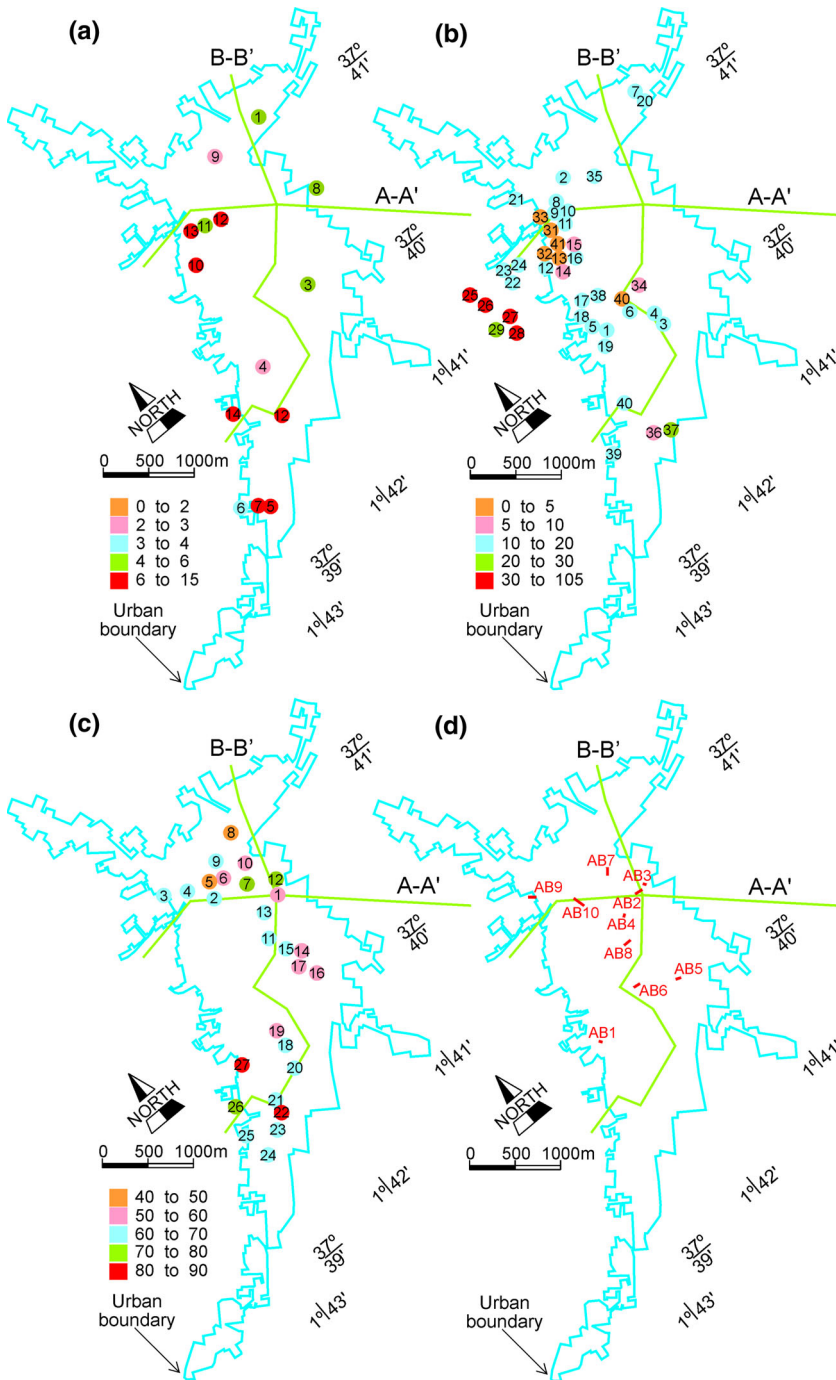
Fig. 2 Geological, geotechnical, and geophysical data from the literature, showing thickness prospected in m; **a** 14 field-ground testing data; **b** 40 mechanical drillings; **c** 27 electrical geophysical tests (IGME 1992); **d** 10 shallow refraction profiles (IGME 1992)

Table 1 Geotechnical classification of geological formations identified in Lorca town (Fig. 1)

Epoch/age	Lithological types [a]	Geological/seismic formation	Thickness (m)	N_{30} (dimensionless)	Real density (g cm^{-2})	A_C (MPa)	V_S (m s^{-1})
Quaternary — Holocene	(1) Cropland, anthropogenic fillings	Human-induced sediments	(31) 0.2–3.3	(5) 4–21			<180
	(2) Alluvial terraces (sand, gravel)	Post-orogenic unconsolidated sedimentary filling	(15) 1.5–21	(23) 6–36	(9) 1.55–1.77		220–380
	(3) Colluvials		(6) 0.6–15.8	(17) 9–41	(3) 1.73–1.97		
Pleistocene	(4) Glacis III	Post-orogenic consolidated sedimentary filling	(18) 2.4–25	(31) 13–59	(2) 1.56–1.89		340–580
	(5) Glacis II		(6) 1.4–15.1	(19) 15–56	(3) 1.76–1.98		
	(6) Glacis I		(6) 4.1–8.6	(12) 28–69			
Tertiary (Neogene) middle–upper Miocene — upper Tortonian	(7) Sandy marls, breccias	Post-orogenic medium-hard bedrock	(3) >5	(7) 65-R[b]			660–800
	(8) Gypsum, marls		(1) >5	(2) R			
middle–upper Tortonian	(9) Marls		(2) >5	(3) R	(1) 1.96		
	(10) Breccias, marls		(2) >5	(1) R			
lower–middle Tortonian	(11) Conglomerates, sandstone, marls		(4) >5	(1) R	(2) 2.34–2.38		
Helvetian / lower Tortonian	(12) Marls, gypsum, sandstone					(7) 2.84–7.85	

Table 1 continued

Epoch/age	Lithological types [a]	Geological/seismic formation	Thickness (m)	N_{30} (dimensionless)	Real density (g cm^{-2})	A_C (MPa)	V_S (m s^{-1})
	(13) Polygenic conglomerates		(4) >10	(1) R		(16) 3.53–9.12	
MC Triassic	(14) Dolomitic limestone	Pre-orogenic hardest bedrock					800– >1,000
Permian	(15) Red clays, slates, quartzite		(1) >10			(1) 13.83	
Devonian-Carboniferous	(16) Phyllite, schist, quartzite					(2) 5.49–18.93	
AC Precambrian-Ordovician	(17) Schist, phyllite, quartzite		(9) >10	(14) 13-R	(1) 2.11		

N_{30} values from SPT, real density, and axial compression strength (A_C) include the range and the number (into parenthesis) of data. The range of S-wave velocity (V_S) for geological/seismic formations was deduced from geotechnical data according to the formulations of Ohta and Goto (1978) for unconsolidated materials and consolidated sedimentary fillings, and Fairhurst and Hudson (1999) and Wang (2001) for hard-rocks *MC* Malaguide complex, *AC* Alpujarride complex, *R* refusal

[a] Codes 1 through 17 for lithological types coincide with those described in Fig. 1

[b] R = refusal for N_{30} according to NCSE-02

hard bedrock, which includes conglomerates, marls, gypsum, sandstones; (3) Pliocene and Pleistocene consolidated glacis and colluvials; (4) Holocene unconsolidated colluvials and alluvial terraces; (5) Holocene human-induced sediments, such as croplands and anthropogenic fillings.

In this classification, the bedrock was defined as 'medium-hard' for post-orogenic Miocene materials and 'hardest' for pre-orogenic pre-Triassic materials. Both types of bedrocks, which outcrop at northern and western areas of the town, were prospected between 10 and 50 m in the centre of the town and from more than 100 m at southeast. The thickness of Plio-Quaternary materials decreases progressively to disappear towards the northern and north-western parts hilly boundaries of the town. The geometry of Plio-Quaternary formations is controlled by a main set of ENE-WSW faults linked to the Alhama de Murcia Fault System, which deepens the bedrocks towards the southeast (Silva et al. 1992), and by a secondary set of NW-SE and SW-NE conjugated normal faults that rises or deepens the basement, compartmentalizing the basin.

3 Geotechnical data

Mechanical and physical properties of unconsolidated sediments and hard-rocks deduced from geotechnical data allow preliminary dynamic seismic response of geological formations (Ohta and Goto 1978; Wang 2001; and references therein). Preliminary S-wave velocity (V_S) values were deduced from normalized 30 cm standard penetration test (SPT) blow counts (N_{30}, hereafter is denoted simply as N), axial compression strength (A_C), real density (D), and maximum shear modulus (G) data compiled from literature and geotechnical reports.

For unconsolidated materials, numerous relations between N and V_S exist in the literature. The most common functional form is $V_S = x \cdot N^y$, being the constants x and y determined by statistical regression of datasets; x and y vary in the 50–150 and 0.1–0.8 range respectively, depending on the geological epoch and depth (for x), and the lithological type (for y). The error of deduced V_S is often less than 20 % (Ohta and Goto 1978; Sykora and Koester 1988; Towhaka and Roteix 1988). Note that refusal (hereafter denoted simply as R; see Table 1) for N_{30} produces when: (1) $N_{15}(15$ cm$) > 50$ strokes, (2) $N_{30} \geq 100$ strokes, or (3) no breakthrough after 10 strokes (Bowles 1988). Data compiled from geotechnical reports follow this criterion according to the NCSE-02.

For hard-rocks, common relations between A_C and V_S have been formulated in the literature. V_S is typically observed to increase as a logarithmic function of A_C, as $V_S = i \cdot Ln(A_C) + j$, being the constants i and j determined by statistical regression of each lithological dataset; for instance, i and j vary in the 500–1,500 range for pre-Triassic carbonate and metapelitic rocks (Paterson 1978; Fairhurst and Hudson 1999; Wang 2001). The error of deduced V_S may be greater than 20 %. Some V_S data have been deduced as $V_S^2 = G/D$, using G data in the $7 \times 10^5 - 5 \times 10^6$ KPa range from literature (e.g. Paterson 1978; Mayne and Rix 1993; Wang 2001).

The above described formulae and the variable-quality data compiled from the literature and geotechnical reports were used to deduce preliminary V_S values (Table 1) for each geological formation identified. For unconsolidated Holocene sediments, V_S was less than 380 ms^{-1}, even less than 180 ms^{-1} for human-induced sediments, such as cropland and anthropogenic fillings (Table 1). For Pliocene and Pleistocene consolidated glacis, V_S was between 340 and 580 ms^{-1} (Table 1). For medium-hard bedrocks, V_S was between 660 and 800 ms^{-1}. For hard bedrocks, V_S was between 800 and 1,000 ms^{-1} for carbonate forma-

tions and greater than $1,000\,\text{ms}^{-1}$ for metapelitic formations (Table 1). These results are in agreement with those found for similar geological formations in the region (e.g. Alcalá et al. 2002; Delgado et al. 2003; Navarro et al. 2007; García-Jerez et al. 2007a, b). The above described V_S values and another 10 empirical V_S values pointed by IGME (1992) from refraction profiles in the uppermost 15 m of the ground were used to improve the geological/seismic conceptual model in areas without geophysical surveys and calibrating the initial V_S estimates deduced from SPAC surveys (see Sect. 4.1).

4 Analysis and results of ambient noise records

4.1 Rayleigh velocity dispersion curves

The shallow geological structure of Lorca town has been studied using a Spatial Autocorrelation method (SPAC). The measurements were carried out at eleven open spaces, hereafter called SP sites (Fig. 1), obtaining Shear-wave velocity profiles from the Rg-wave dispersion curves by means of inversion procedure.

Vertical components of ground motion, excited by ambient noise, were recorded at the surface using circular-shaped arrays. Five high-sensitivity VSE-15D sensors surrounding a sixth central sensor with same characteristics and a SPC-35 digitizer were used. These devices provide an acceptable response for frequencies (f) ranging from 0.25 to 70 Hz. The radii (R) ranged from 3 to 50 m. Different radii were used depending on the thickness of geological formations deduced from geological and geophysical data and on the dimensions of the open areas. Recording time was 30 min, and the signal was sampled with a rate of 100 samples per second (sps). All records were analysed by using an implementation of the SPAC method (Aki 1957). In order to obtain the correlation coefficient $\rho(f, R)$, the cross-correlations between records on the circle and the central station were calculated in frequency domain and divided by the autocorrelation at the center. The correlation coefficient was separately computed for a set of overlapping time windows and subsequently plotted as a function of time and frequency. The time windows used were 20 s long with an overlapping of 80 %. The stability of $\rho(f, R)$ was checked for the set of time windows and those with anomalous values of $\rho(f, R)$ were not considered. Finally, the phase-velocity of the Rg-wave, $c(f)$, was computed for each frequency using Eq. (1), and applying a polynomical fit of the ρ versus f relation (Fig. 3).

$$\rho(f, R) = J_0 \left(\frac{2\pi f}{c(f)} R \right) \tag{1}$$

where J_0 represents the zero-order Bessel function.

The frequencies of the obtained curves ranged from 2.9 to 24.0 Hz and the phase velocity values varied between 184 and 749 m s^{-1} (Table 2).

4.2 Inversion of S-wave profiles

Rg-wave phase velocities have been used in order to obtain shear-wave velocities, V_S. As it is well known, most of iterative inversion methods require building up a proper initial ground model. Since there were serious uncertainties on the thickness and stiffness of geological formations in some scarce-data areas of Lorca town, and in order to minimize the dependence on the initial model, a hybrid inversion scheme has been carried out in this work. The employed algorithm consisted of a simple random search in the model space combined
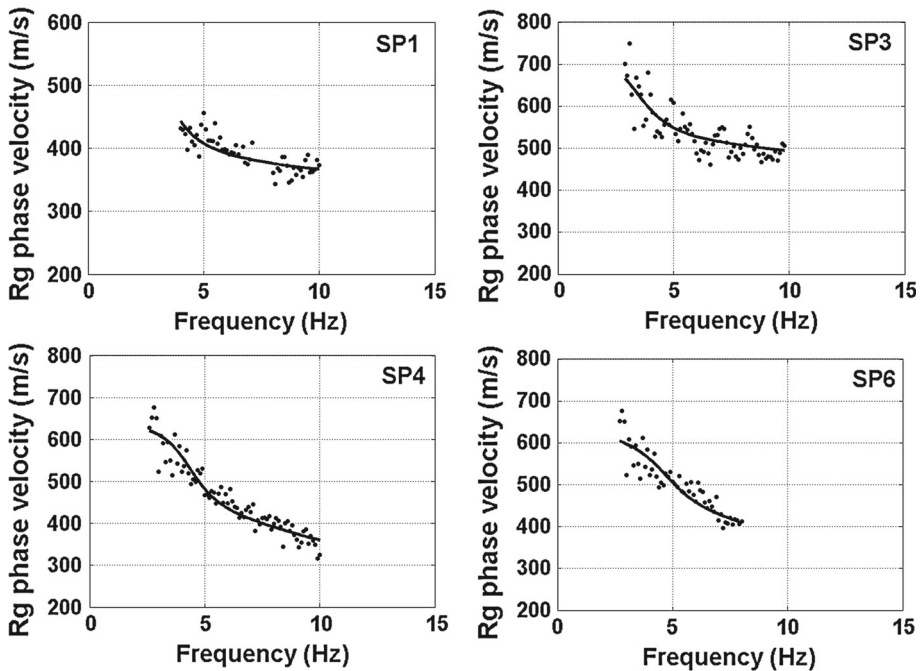
Fig. 3 Examples of Rg-wave phase velocities (*black points*) measured at different places (see Fig. 1). *Solid lines* represent the fundamental-mode Rg dispersion curves corresponding to the 1D ground models obtained from the inversion process

Table 2 Characteristics of the array setup, dispersion curves, and S-wave velocity models at the array sites

Spac	Δf (Hz)	Δc_R (m s^{-1})	ΔV_S (m s^{-1})	V_S^{30} (m s^{-1})
SP1	4.0–10.0	343.5–456.3	378.0–704.1	395.4
SP2	10.5–24.0	225.1–694.2	204.7–1223.0	522.3
SP3	2.9–9.8	461.3–749.1	221.7–789.5	452.5
SP4	2.6–10.0	316.3–676.7	373.7–700.3	404.5
SP5	6.1–10.0	551.4–741.5	263.6–742.6	552.0
SP6	2.7–8.0	396.8–676.7	292.6–706.0	388.1
SP7	11.2–19.7	362.6–582.0	366.7–800.1	536.1
SP8	3.3–15.5	325.3–552.0	343.4–661.8	411.0
SP9	4.5–10.0	268.7–453.6	236.9–578.3	333.9
SP10	4.1–19.0	183.6–480.1	175.5–567.1	327.1
SP11	3.7–30.9	349.6–623.4	350.6–710.6	453.7

Δf—Frequencies ranging.
Δc_R—Phase-velocity ranging of the Rayleigh-wave
ΔV_S—Shear-wave velocity ranging
V_S^{30}—Average shear-wave velocity from the uppermost 30-m ground thickness

with a local optimization algorithm (Simplex-Downhill method). The successive application of these methods allowed an extensive sampling of the models space and a high refinement around the good-fitting models. An implementation of this algorithm suitable for parallelized computation (García-Jerez et al. 2007b; Luzón et al. 2011) has been applied in order to deal with the computational cost. A master processor generates a random set of 100 initial models inside defined ranges of the ground parameters, obtained from the previous geological and

geotechnical data, and distributes them to the cluster. Then, 100 iterations using the local optimization algorithm around such models were carried out by the other CPUs.

Because of the large differences among the dispersion curves, both in frequency and in phase velocities, the number of layers and range for thicknesses and shear velocities were different for each SPAC site. Examples of the shear-wave velocity profiles obtained are shown in Fig. 4. A smooth profile derived directly from the dispersion curve (that is, without defining a discrete set of model parameters) has been shown for reference with black points. It is based on the rough approximations of effective sampling depth of $\lambda/3$ for Rayleigh waves of wavelength λ, and shear wave velocity at that depth of about 110 percent of the phase velocity (e.g. Tokimatsu 1997). Finally, the average shear-wave velocity of the uppermost 30 m (V_S^{30}) has been finally computed for each model (Table 2). Note that the vertical distributions of elastic properties (i.e. the original profiles) are still necessary for accurate evaluation of ground amplifications. A detailed analysis of the behaviour of these
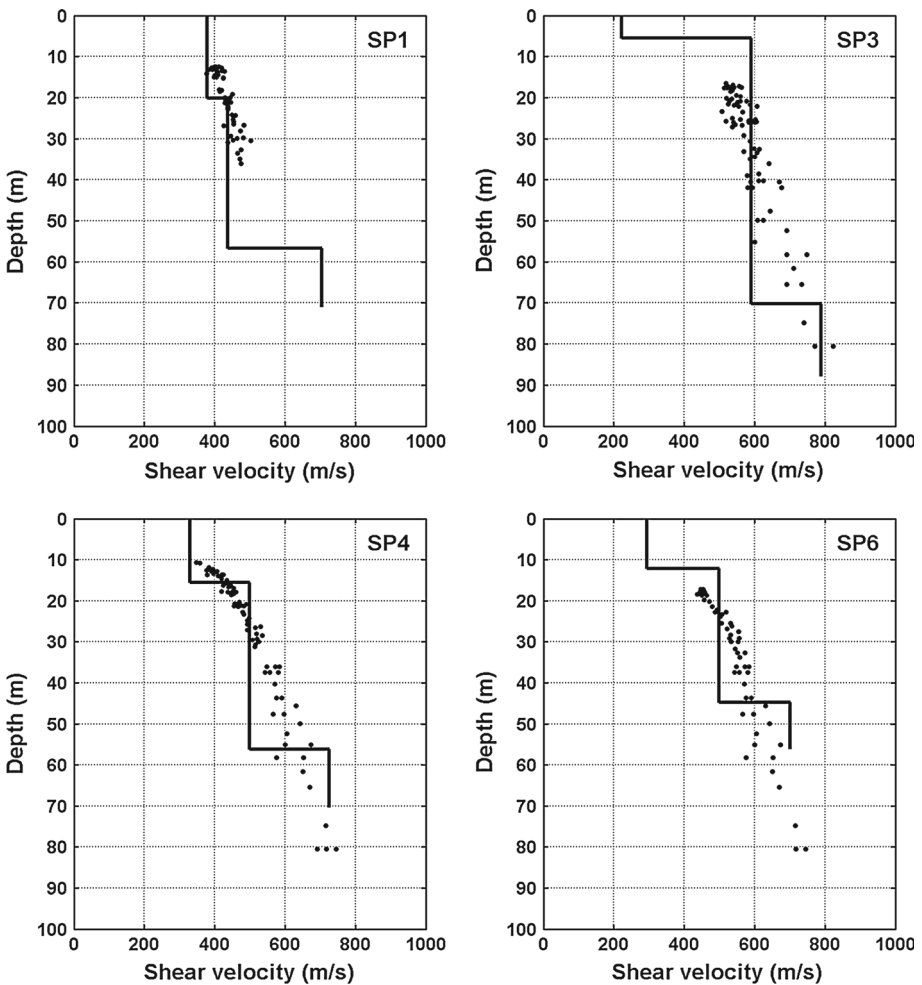
Fig. 4 Examples of Shear-wave velocity models derived from inversion of phase velocities in different places of Lorca town

ground structures under the May 11, 2011 earthquake (Mw = 5.2) has been carried out by Alcalá et al. (2013).

4.3 Computation of HVSR and predominant period

The measurements of ambient vibration in Lorca town were performed during March 2004 and complemented in June 2011 to evaluate the resonant period of the shallow geology. Two portable velocity sensors, similar to those used in the array measurements, were employed. Three-component ambient vibrations were recorded at 82 sites of a 400 m × 400 m grid. The observation time was 180 s and the signal was sampled with a rate of 100 sps. The records were performed at daytime as far from traffic and artificial sources of noise as possible. Since ambient vibration spectra could be more or less influenced by close sources, Fourier spectra were calculated at each point for several time windows free of artificial disturbances. Nakamura's method (Horizontal-to-Vertical Spectral Ratio, HVSR; Nakamura 1989) was applied to obtain the predominant period of each site (Fig. 5).

The shorter predominant periods were less than 0.15 s for the pre-Triassic hard-rock sites at the north and southwest of the town (Fig. 6). The Miocene medium-hard rock sites at the north and northeast provided values between 0.15 and 0.3 s. At the northern and western hilly urban boundaries, the Pliocene and the older Pleistocene glacis formations showed values in the 0.2–0.5 s range. The predominant periods were larger than 0.5 s for the latest Pleistocene glacis formations and the Holocene alluvial fan deposits from the Guadalentin River in the centre and eastern parts of the town. Associated with the recent human-induced sediments, the highest periods up to 0.8 s were found in the centre on the town and in the southeast fertile plain (Fig. 6). The urban area exhibits large spatial variability in terms of HVSR shape. Moreover, multiply peaked HVSR are often found in this area, with the predominant peak depending on the local impedance contrasts. These characteristics reflect the complexity of the local shallow structure.
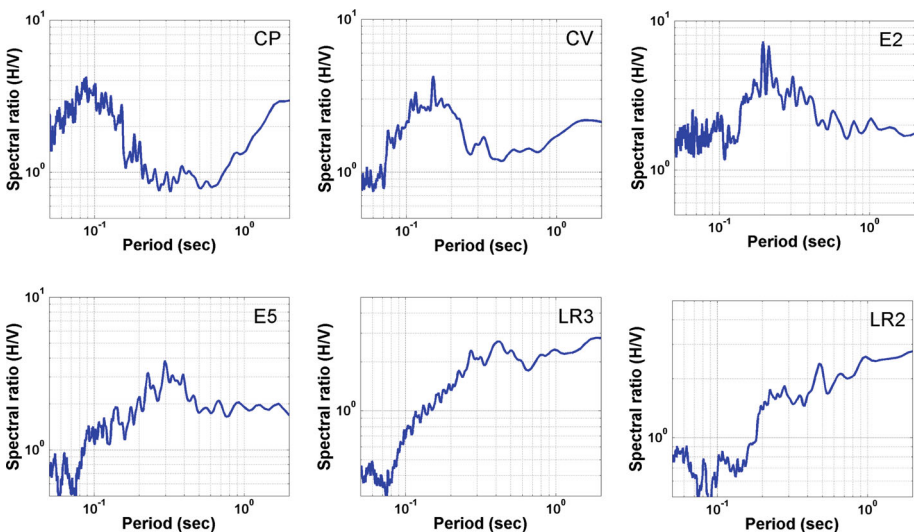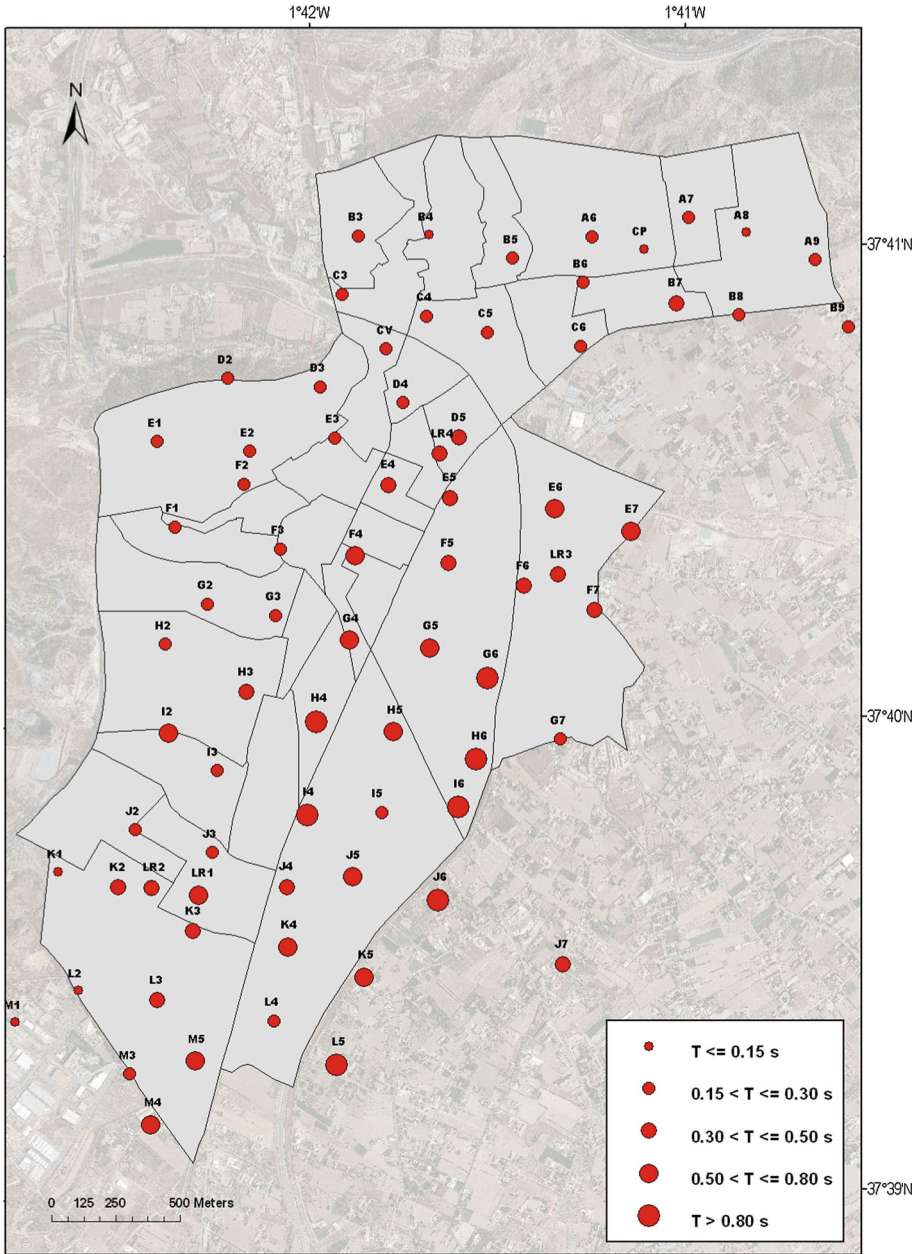

Fig. 5 Examples of spectral ratio in different places of Lorca town with different soil conditions

**Fig. 6** Ground predominant period spatial distribution at Lorca town from ambient noise HVSR method

5 Site amplification

An elemental local array composed of 3 strong-motion stations (ETNA-KINEMETRICS) was deployed in different parts of Lorca town from March 2004 to October 2008 to obtain information on the ground motion amplification due to local geological conditions. The stations

(LRC1-3; Fig. 1) were distributed at sites with different geology. LRC1 station was located at Lorca Castle, close to SPAC point SP5 (Fig. 1) over Miocene medium-hard bedrock (Table 1). This station has been considered as reference station for this analysis. LRC2 station was located in the local Urban Planning Office, close to SPAC point SP7 (Fig. 1), the borehole 10 (Fig. 2b), and the CV point (Fig. 6). LRC3 station was located in the headquarters of local Civil Protection Office, close to SPAC point SP2 (Fig. 1), the field-ground testing 1 (Fig. 2a), and the CP point (Fig. 6). Both LRC2 and LRC3 stations are placed over Pleistocene glacis (Fig. 1).

Since its completion, this array has recorded 23 local earthquakes with magnitudes between 1.4 and 5.5 (Richter scale). An example of the recorded acceleration time histories is shown in Fig. 7. It corresponds to an earthquake close to Mazarron town (Murcia) with
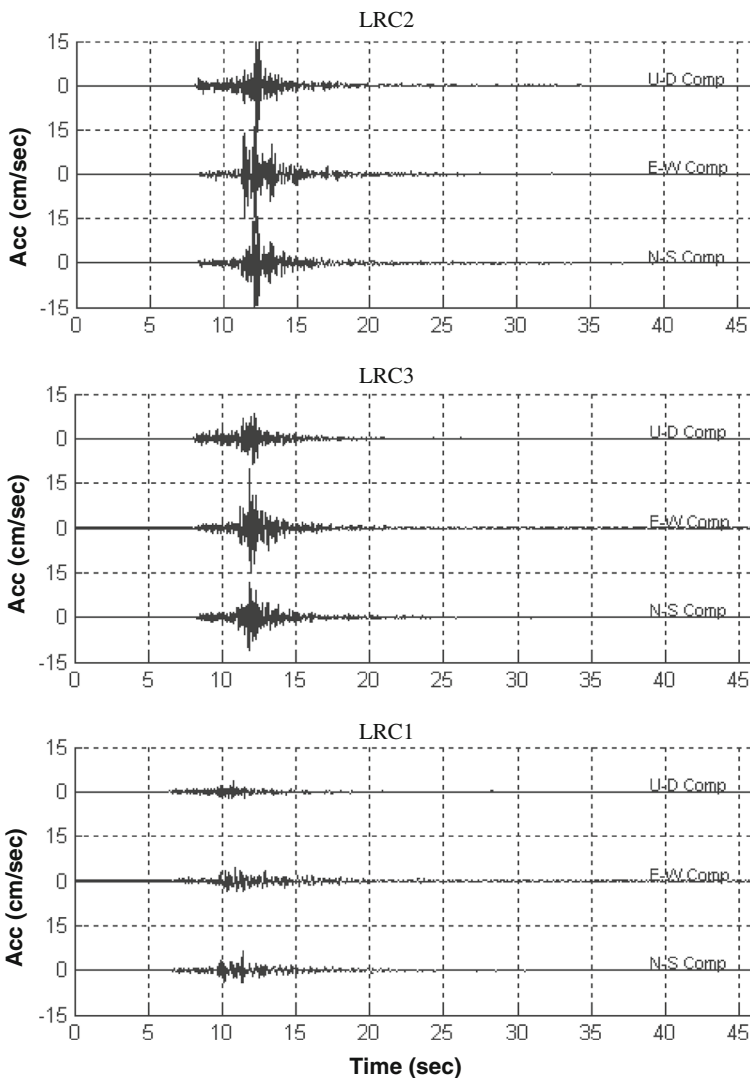
Fig. 7 Example of simultaneous recorded acceleration time histories in Lorca town from an earthquake occurred near Lorca ($m_b = 3.7$ and epicentre distance 25.8 km)

body wave magnitude $m_b = 3.7$ and epicentre distance 25.8 km to Lorca town. The results show clear differences in the level of amplification.

Fourier spectra were calculated using a time window containing S and coda waves, and the classical spectral ratios between the stations over Pleistocene glacis and the reference station were calculated (Fig. 8). The spectral amplification bands obtained from classical spectral ratio SSR and from HVSR of ambient noise are quite similar (Fig. 9). The different average amplifications obtained from these techniques at frequencies below about 1 Hz evidence instability or larger statistical uncertainties in this band. In particular, this kind of perturbations in the HVSR may be due to wind, meteorological events or insufficient sensitivity of the seismometers, among other causes, as reported by SESAME (2004). Amplifications derived from the classical spectral ratio are considered to be the most reliable result in case of discrepancy. The average amplification at LRC2 station is around three in the band from 0.1 to 0.2 s. The LRC3 station shows an average amplification of four for the periods less than 0.1 s.

6 The 2011, Mw 5.2 Lorca earthquake

The mainshock of the Lorca seismic series, occurred on May 11th at 16:47 UTC (18:47 local time) with epicentral distance of 5.5 km from the city center, had moment magnitude 5.2 and shallow hypocenter (4.6 km deep). A PGA of 0.37 g and peak ground velocity (PGV) of 35.4 cm/s were observed by the Instituto Geográfico Nacional (IGN; www.ign.es) at the Lorca strong-motion station. The maximum macroseismic intensity was initially estimated as VII (EMS-98 scale) by the IGN (IGN 2011) and the Instituto Andaluz de Geofísica (IAG 2011; www.ugr.es/~iag). This event had a relevant foreshock with Mw = 4.6 and maximum intensity VI two before (15:05, UTC), as well as a Mw 3.9 aftershock four hours later (20:37 UTC). It was followed by more than one hundred aftershocks during the first month, 80 % of them during the first week.

This relatively small event caused in Lorca an outwardly disproportionate impact: 9 casualties, near 300 injured, one RC building and some masonry constructions collapsed, 1,018 buildings (15.8 %) officially declared with structural damage (329 of them to be demolished), and 1,328 buildings with slight structural damage and/or moderate non-structural damage (20.7 %) that need to be repaired before being used. Other 4,035 buildings (62.9 %) experienced minor or negligible damage and were classified as inhabitable (Fig. 10). Cultural heritage buildings were also seriously damaged, especially religious ones. The roof and Cupola of the Santiago church collapsed completely, whereas other churches and a tower of the Lorca Castle suffered serious structural damage.

There were damaged buildings in all districts of the town, but the levels and percentages were fundamentally different depending on building vulnerability and ground motion characteristics. The most severe damage appears in La Viña (southwestern zone) and La Alberca and La Alameda districts, both lasts close to the Guadalentin River (Fig. 10). Particular attention has to be paid to this observed spatial distribution of damage and its relation with spatial differences of ground motion level and frequency content. Local intensity differences obtained from macroseismic data and ground motion parameters at several places reflect the influence of unconsolidated Quaternary formations on damage distribution.
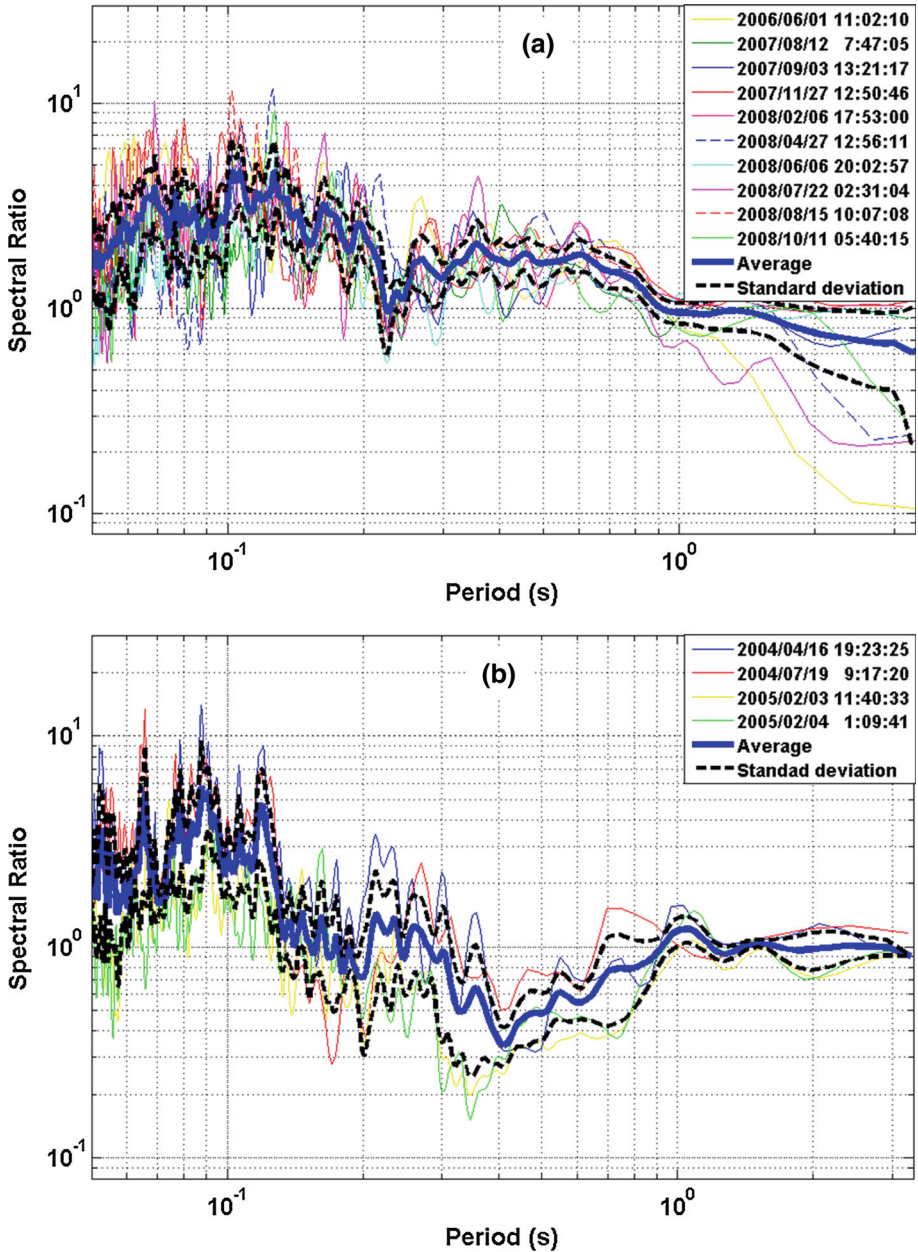
Fig. 8 Average spectral amplifications obtained from classical spectral ratios (*solid-bold blue lines*) and standard deviation (*solid-dotted black line*). **a** LRC2 station; **b** LRC3 station

7 Discussion

The progressive assimilation of geological, geotechnical, and geophysical data from the literature and geotechnical reports (Fig. 2), as well as the seismic surveys performed, has
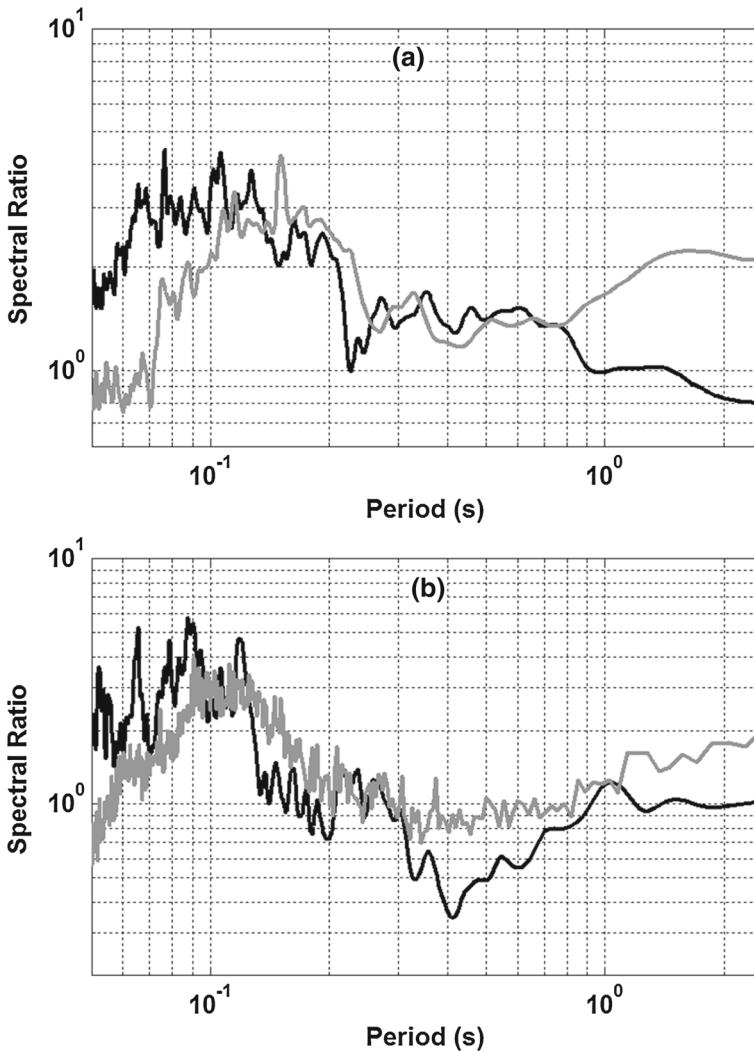
Fig. 9 Comparison between calculated transfer function by using classical spectral ratios (*black line*), and HVSR of ambient noise (*gray line*). **a** LRC2 station; **b** LRC3 station

helped us to improve the geological definition, validating or rejecting new information, and supplying suitable places for SPAC surveys, which in turn served to improve the geological conceptual model.

SPAC method has shown good performance in Lorca town, providing new insights into the shallow sedimentary structure in this area. Due to the range of velocities and depths down to the geotechnical basement, the small aperture arrays easily deployed in the urban area were enough to provide new data of the S-wave velocity structure at depths larger than those reached by the previously existing geotechnical and active seismic surveys. The spectral power of ambient noise in the band of interest was high enough to allow retrieving good quality dispersion curves.
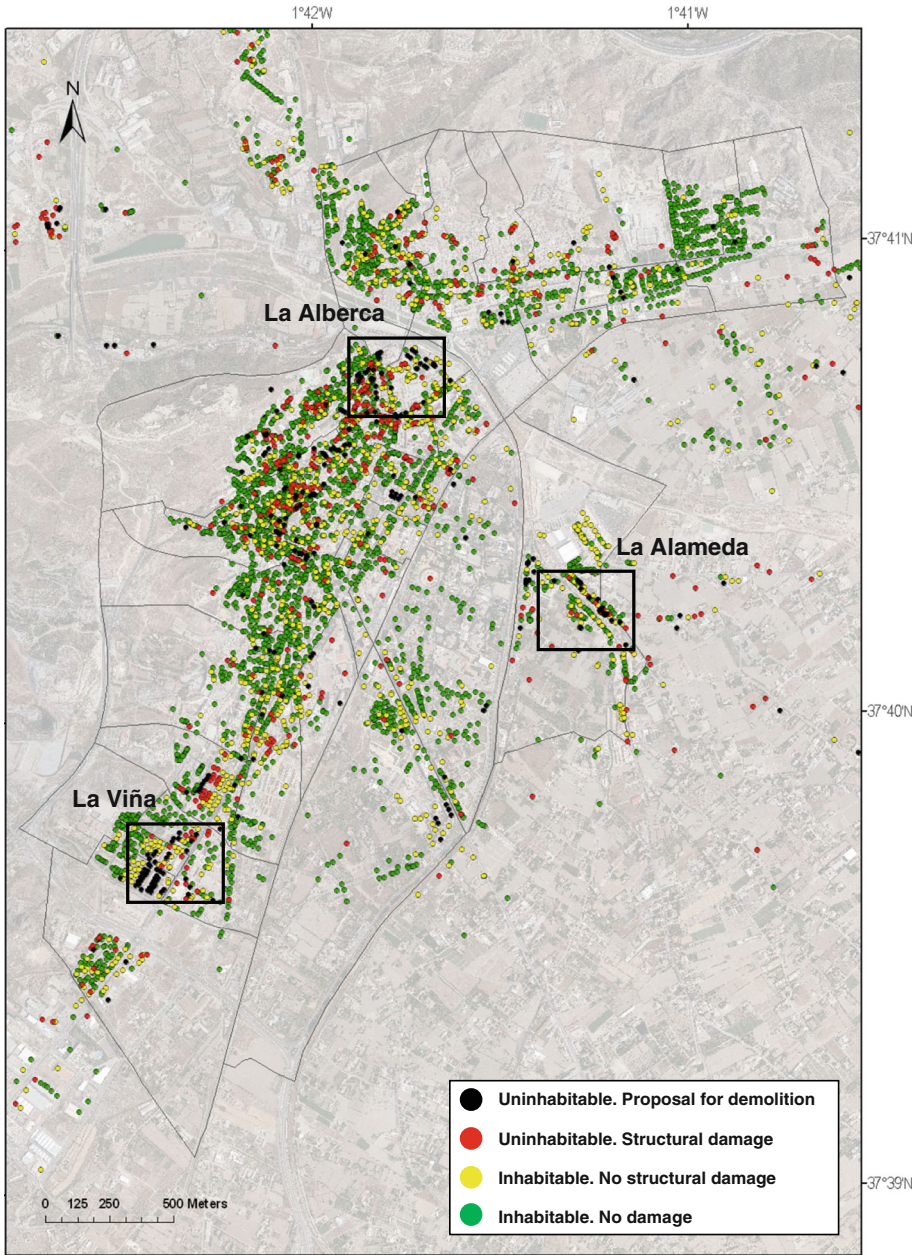
Fig. 10 Damage distribution in Lorca town due May 11th, 2011 Lorca earthquake

As a main contribution for the seismic microzonation of Lorca town, a new geological mapping at scale 1:10,000 allows geometrical definitions of the geological formations, especially the Plio-Pleistocene glacis sequences and the Holocene alluvial and colluvial formations. Two geological cross-sections show the geometrical interpretation of the complex
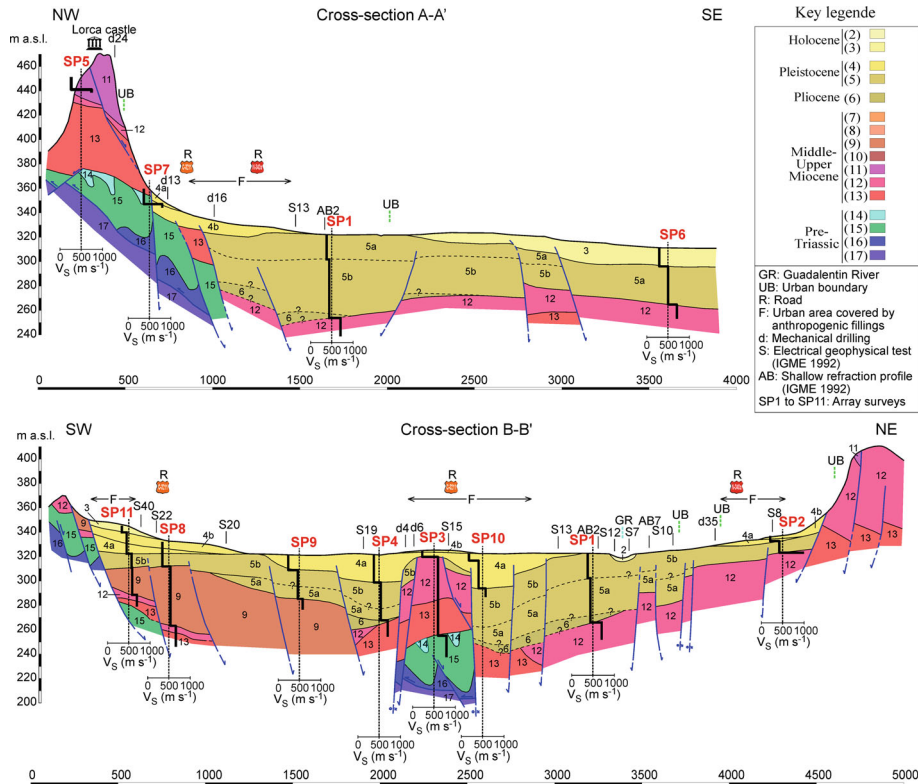
Fig. 11 Geological/seismic cross-sections *A-A′* and *B-B′* at scale 1:10,000 (see location in Fig. 1) inferred from geological mapping (Fig. 1; Table 1), geotechnical data, electrical geophysical test, shallow refraction profiles (Fig. 2), and SPAC surveys. S-wave velocity (V_S) models derived from array measurements of ambient noise (*SP1* to *SP11* in Fig. 1, V_S in m s^{-1}) were also used

sedimentary record (Fig. 11), which in turn determines the high heterogeneity in V_S values and predominant periods over short distances observed in the urban area.

The accurate geological definition allows extend seismic information to scarce-data areas with similar geological materials. For instance, the identification of local-scale geological heterogeneities was essential to define proper V_S^{30} values and the contrast between bedrocks and unconsolidated sediments potentially subjected to amplification during a seismic event (Fig. 12).

The 17 geological formations identified in Lorca town (Fig. 1; Table 1) have been clustered into 5 main geological/seismic formations attending to their seismic behaviour, as following:

(1) The first seismic formation includes those punctual zones where conditions for EC8-D ground class have been found or could be present (Fig. 12), as deduced from geological mapping (Fig. 1) and geotechnical data (Table 1). V_S^{30} values are less than 180 m s^{-1} for those checked areas in the historic district of the town. This formation includes the geological formation 1 (Table 1): cropland and anthropogenic fillings of variable thickness overlaying Pleistocene glacis.

(2) The second seismic formation includes those zones where conditions for EC8-C ground class have been found (Fig. 12). V_S^{30} values vary in the 220–380 m s^{-1} range. This formation
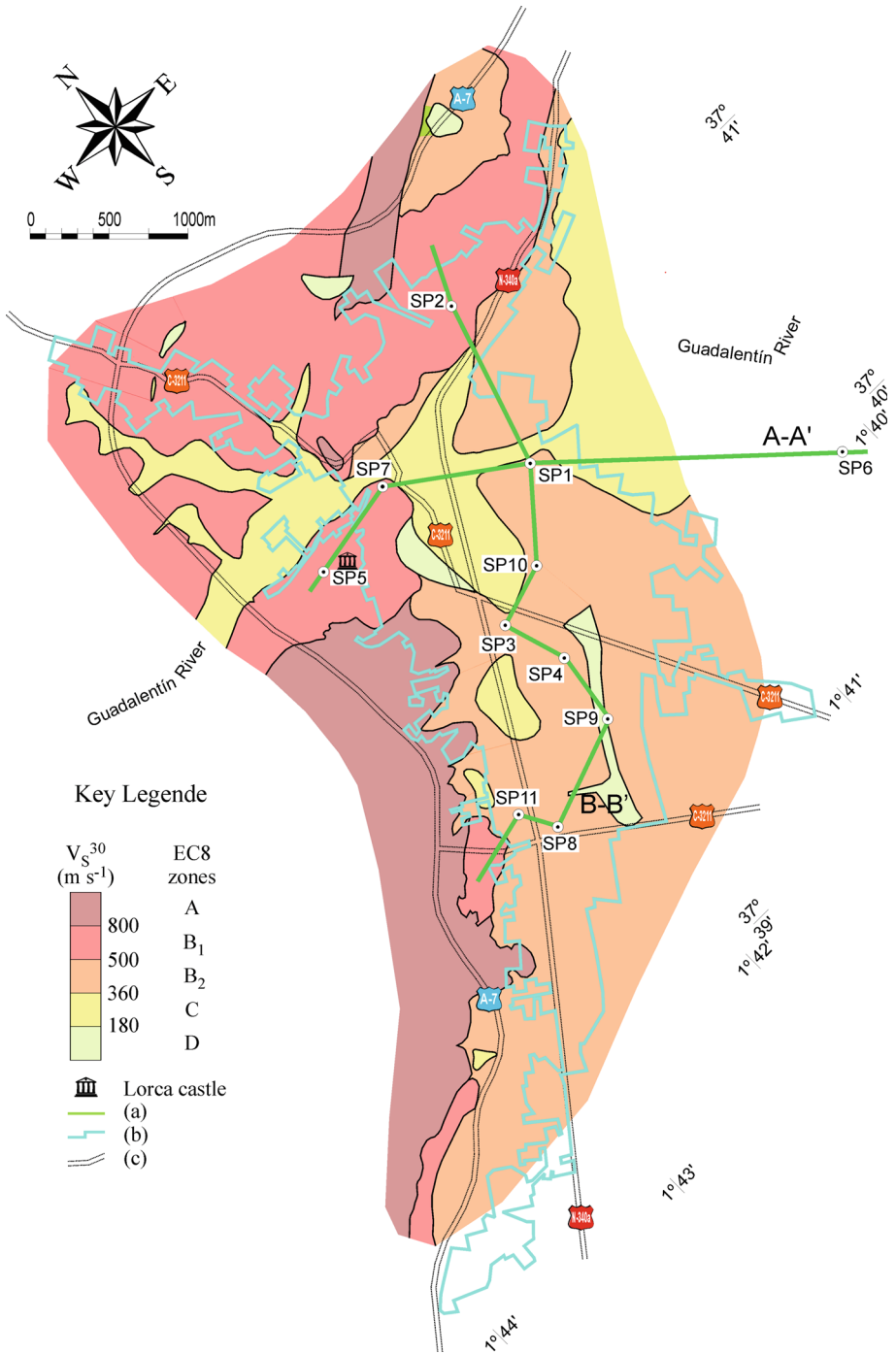
Fig. 12 Soil classification map of Lorca town based on the average shear-wave velocity distribution down to 30 m (V_S^{30} in m s^{-1}), according to Eurocode No. 8 (1998). **a** Geological cross-sections A-A' and B-B' and array SP1 to SP11 locations, **b** urban boundary (*solid-bold blue line*), **c** main roads

includes mainly geological formations 2 and 3: unconsolidated Holocene colluvials and alluvial terraces belong to the Guadalentin River valley (Table 1).

(3) Attending to the range of V_S^{30} values stated by the EC8 (1998), a large area of Lorca town covered by geological formations 4–6 (i.e. the three generations of Pliocene-Pleistocene consolidated glacis; Table 1) and geological formations 7–13 (i.e. the lower-to-upper Tortonian post-orogenic medium-hard bedrock: Table 1) meet the requirements to be classified into the B ground-class. Due to the variety of geological/seismic conditions and ranges of V_S involved, an internal division has been proposed in order to segregate the consolidated glacis from the lower-to-upper Tortonian formations. The Pliocene and Pleistocene glacis have been classified here as the third seismic formation B_2 (Fig. 12), with V_S^{30} values in the 340–580 m s^{-1} range. The lower-to-upper Tortonian post-orogenic medium-hard bedrock have been classified here as the fourth seismic formation B_1 (Fig. 12), with V_S^{30} values in the 660–800 m s^{-1} range. In addition, the spectral amplification factors between formations B_2 and B_1 obtained from strong motion records are up to 5 in the short period range (Fig. 9), supporting the internal division performed.

(4) Finally, a fifth seismic formation has been defined for those areas where conditions for EC8-A ground class have been found (Fig. 12). V_S^{30} values vary in the 800–1,000 m s^{-1} range for pre-orogenic Triassic carbonate hardest bedrock (geological formation 14; Table 1) and it is greater than 1,000 m s^{-1} for pre-Triassic metamorphic hardest bedrock (geological formations 15–17 from the Alpujarride and Malaguide Complexes; Table 1).

A seismic microzonation of Lorca town has been proposed in terms of the fundamental ground predominant period distribution of surface geology deduced from the ambient noise HVSR method (Fig. 6). Periods vary from 0.1 to 1.0 s and show an overall trend to increase as the thickness of Quaternary formations increases from the northern and western hilly rocky areas to the central and eastern sedimentary zones. The range of ground predominant periods is a key issue for civil engineering, since it affects the building typologies found in Lorca (buildings between one and 13 stories). A detailed study of the natural periods of RC buildings in Lorca Town has been performed by Vidal et al. (2012), who have found a relationship T = 0.054 N before the May 11th, 2011 Lorca earthquake and a relationship T = 0.075 N considering buildings with different damage levels, where T is the natural period and N is the number of stories of the building.

In order to identify those sites where ground predominant period and natural period of existing buildings are close, the storey numbers of stock of buildings in Lorca and its natural period deduced from the first relationship mentioned above have been plotted in Fig. 13. By comparing Figs. 13 and 6 it is possible to recognize sites where soil-building resonance phenomena may have been relevant. A comparison of these figures with Fig. 10 could aid to get an overall idea of where resonance may exist and this phenomenon might have had certain relevance in earthquake damage. In particular, the heavily damaged district of La Alberca shows ground predominant periods in the 0.15–0.3 s range. This area is characterized by its great constructive heterogeneity, existing buildings with different typologies, age and number of stories (between 1 and 6). This last feature indicates that the natural periods are below 0.3 s and accordingly in the resonance range for some particular buildings.

La Viña district was the urban area with more severe damage. This zone presents ground predominant period values between 0.15 and 0.5 s. The constructive typology consists of RC buildings of 4–6 stories and natural periods ranging between 0.22 and 0.32 s. This fact also points out that certain buildings may come into resonance.
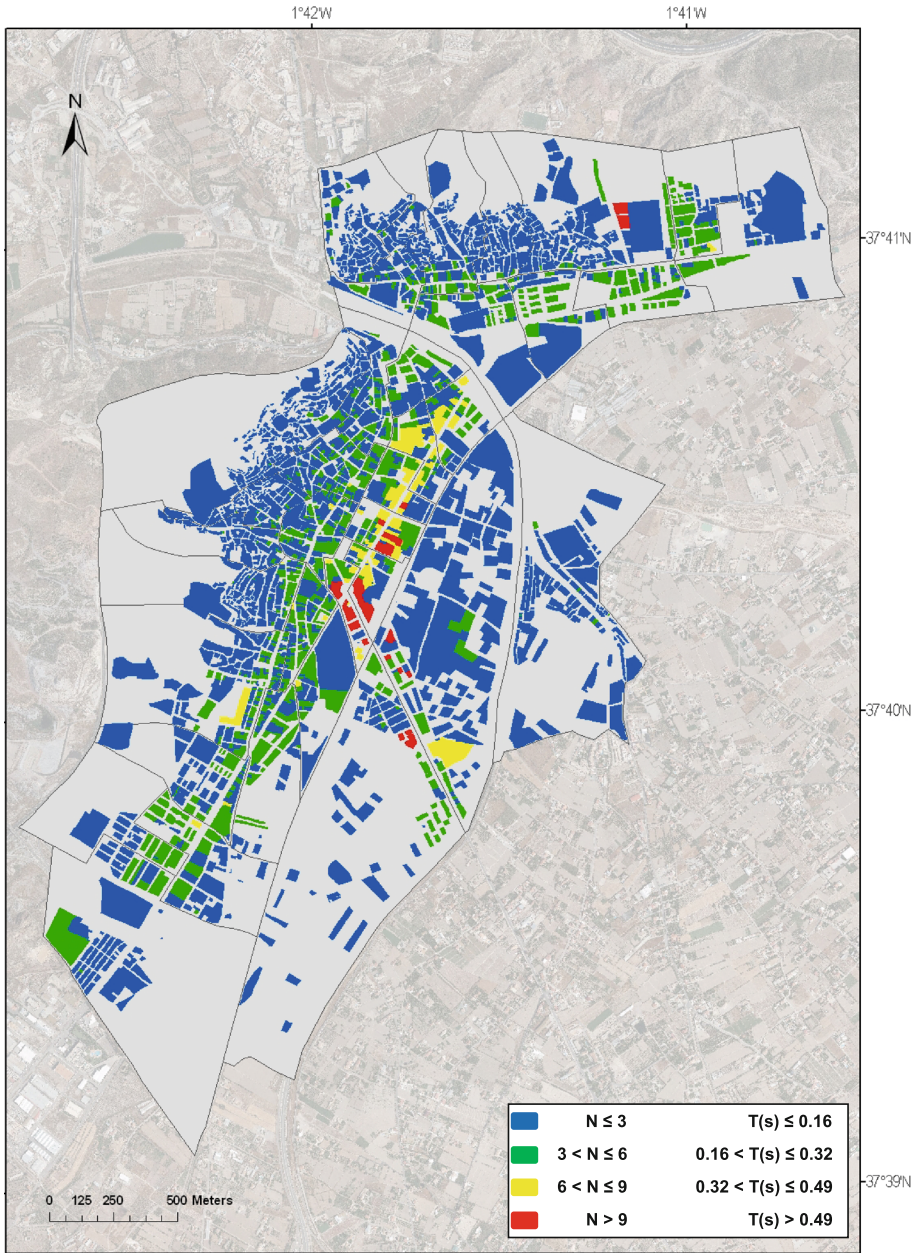
Fig. 13 Storey number (*N*) distribution of existing RC buildings in Lorca town and its corresponding natural period (*T*)

The Alameda zone presented extensive damage in buildings with less than 4 stories (T $\leq$ 0.16 s), whereas the ground predominant period in this zone is ranging between 0.3 and 0.8 s. From these results it is inferred that soil-building resonance phenomena was not a defining characteristic of the damage distribution in this area.

8 Conclusions

Geological mapping at scale 1:10,000 is a basis for the predictable seismic microzonation of Lorca town. The shear-wave velocity structures obtained by means of inversion of Rayleigh wave dispersion data at each SPAC site are in good agreement with the geological structure. As shown in Fig. 11, at least four SPAC sites (1, 4, 6 and 8) show V_S values less than $500 \, \mathrm{m \, s^{-1}}$ for prospected thickness up to about 50 m. In the other sites, this velocity is reached at shallower depth. V_S^{30} values allow the interpretative seismic zonation of Lorca town. Four sites have $V_S^{30} < 400 \, \mathrm{m \, s^{-1}}$ and only three sites are between 522 and $552 \, \mathrm{m \, s^{-1}}$ (Table 2).

Geological materials have been clustered into 5 geological/seismic formations according to the V_S^{30} ranges proposed by the different ground classes defined by the Eurocode 8 (EC8 1998). For this aim, the V_S^{30} values obtained from SPAC surveys were complemented with V_S values from shallow refraction profiles (IGME 1992), V_S values deduced from N_{30} and A_C data, and the thickness of geological formations (Table 1; Fig. 11). The most widespread EC8 soil type is B2 followed by B1 (Fig. 12). Class C also covers a significant part of the urban area.

The seismic microzonation map of Lorca town in terms of ground predominant period (Fig. 6) reflects rough differences between hard ground areas (lower predominant period values) and less hard zones (higher values) as well as the general trend of periods to grow as the thickness of Quaternary formations increases.

Although the distribution of damaged buildings in Lorca town is widespread in all districts of the town, but with different levels and percentages, damage is specially concentrated in areas where predominant periods of soil are between 0.15 and 0.8 s. (e.g. La Viña, La Alberca, and La Alameda districts).

The energy input spectra of ground motion, obtained convolving the transfer functions derived from SPAC 1-D models (SP in Fig. 1) with the record obtained at Lorca IGN station (Alguacil et al. (2013)), clearly shows that most of the energy supplied by the shaking was in the range 0.3–0.6 s. In this period range, a pseudo-velocity level of $100 \, \mathrm{cms^{-1}}$ was exceeded. Considering the natural period range of RC buildings (Vidal et al. 2012), the mean seismic demand was quite high for buildings with more than 3 stories at these places. From these results, it is possible to infer the influence of site effects on the damage distribution in Lorca town.

The relatively large ground motion amplitude (0.377 g on rock and higher in soils) and likely soil-building resonances at several sites increased the level of damage. On the other hand, the small relative significant duration (RSD) of energetic phases of the May 11th shaking (∼1 s) probably reduced the consequences of the resonance effect. It should be remarked that the frequency content of the earthquake (shown by LOR station record located at hard soil conditions) and the vulnerability of buildings also played a major role in the damage distribution.

References

Alcalá FJ, Espinosa J, Navarro M, Sánchez FJ (2002) Propuesta de división geológica regional de la localidad de Adra (provincia de Almería). Aplicación a la zonación sísmica. Revista Sociedad Geológica España 15:55–66

Alcalá FJ, Guerrera F, Martín-Martín M, Raffaelli G, Serrano F (2013) Geodynamic implications derived from Numidian-like distal turbidites deposited along the Internal-External Domain Boundary of the Betic Cordillera (S, Spain). Terra Nova. doi:10.1111/ter.12014

Alfaro P, Andreu JM, Delgado J, Estévez A, Soria JM, Teixido T (2002) Quaternary deformation of the Bajo Segura blind fault (Eastern Betic Cordillera, Spain) revealed by high-resolution reflection profiling. Geol Mag 139(3):331–341

Alguacil G, Vidal F, Navarro M, García-Jerez A, Pérez-Muelas J (2013) Characterization of earthquake shaking severity at different sites of Lorca town for the May 11th, 2011 event. Bull Earthq Eng. In this issue

Aki K (1957) Space and time spectra of stationary stochastic waves, with special reference to microtremors. Bull Earthq Res Inst 35:415–456

Aranda C, Vidal F, Alguacil G, Navarro M, Carvallo JF (2012) Damage analysis due to 2010 Chilean earthquake in Viña del Mar residential buildings. 15th world conference on earthquake engineering, Lisbon, p 7

Ashford SA, Sitar N, Lysmer J, Deng N (1997) Topographic effects on the seismic response of steep slopes. Bull Seismol Soc Am 87(3):701–709

Bakir S, Sukuoglu H, Yilmaz T (2002) An overview of local site effects and the associated building damage in Adapazari during the 17 August 1999 Izmit earthquake. Bull Seismol Soc Am 92(1):509–526

Barka A (1999) The 17 August 1999 Izmit earthquake. Science 285:1858–1859

Benito B, Capote R, Murphy P, Gaspar-Escribano JM, Martínez-Díaz JJ, Tsige M, Stich D, García-Mayordomo J, Jiménez ME, Insua-Arévalo JM, Alvarez-Gómez JA, Canora C (2006) An overview of the damaging and low magnitude Mw 4.8 La Paca earthquake on 29 January 2005: context, seismotectonics, and seismic risk implications for Southeast Spain. Bull Seismol Soc Am 97:671–690

Benito B, Navarro M, Vidal F, Gaspar-Escribano J, García MJ, Martínez-Solares JM (2010) A new seismic hazard assessment in the Region of Andalusia (Southern Spain). Bull Earthquake Eng 8:739–766

Bousquet JC (1979) Quaternary strike-slip faults in southeastern Spain. Tectonophysics 52:277–286

Bowles JE (1988) Foundation analysis and design, 4th edn. McGraw-Hill, New York City

Cucci L, Tertulliani A (2011) Clues for a relation between rotational effects induced by the 2009 Mw 6.3 L'Aquila (Central Italy) earthquake and site and source effects. Bull Seismol Soc Am 101(3):1109–1120

Delgado J, Alfaro P, Andreu JM, Cuenca A, Doménech C, Estévez A et al (2003) Engineering-geological model of the Segura River flood plain (SE Spain): a case study for engineering planning. Eng Geol 68:171–187

Dobry R, Borcherdt RD, Crouse CB, Idriss IM, Joyner WB, Martin GR, Power MS, Rinne EE, Seed RB (2000) New site coefficients and site classification system used in recent building seismic code provisions. Earthq Spectra 16:41–68

Egeler CG, Rondeel HE, Pignatelli R (1981) Geological Map of Spain 1:50,000, sheet no. 953 (Lorca). IGME, Madrid

Eurocode No.8 (1998) Design of structures for earthquake resistance. Commission of the European Communities. Doc CEN/TC250/SC8/N335

European Macroseismic Scale (1998) Conseil de L'Europe. In: Grunthal G (ed) Cahiers du Centre Européen de Géodynamique et de Séismologie, vol 15. Luxembourg

Fairhurst CE, Hudson JA (1999) Draft ISRM suggested method for the complete stress-strain curve for intact rock in uniaxial compression. Int J Rock Mech Min Sci 36:279–289

García-Hernández M, López-Garrido AC, Rivas P, Vera JA (1980) Mesozoic paleogeographic evolution of the External Zone of the Betic Cordillera. Geol Mijnbouw 59:68–155

García-Jerez A, Navarro M, Alcalá FJ, Luzón F, Pérez-Ruíz JA, Enomoto T, Vidal F, Ocaña E (2007a) Shallow velocity structure using joint inversion of array and H/V spectral ratio of ambient noise: the case of Mula Town (SE Spain). Soil Dyn Earthq Eng 27:907–919

García-Jerez A, Navarro M, Luzón F, Pérez-Ruiz JA (2007b) Obtención de modelos de velocidad de onda S a partir de las características de las ondas superficiales mediante combinación paralelizada de métodos iterativos de minimización local y métodos de búsqueda aleatoria. In: Proceedings Tercer Congreso Nacional de Ingeniería Sísmica, pp 504–512

García-Jerez A, Luzón F, Navarro M (2008) Determination of the elastic properties and the depth of shallow sedimentary deposits applying a spatial autocorrelation method. Geomorphology 93:74–88

Garcia-Jerez A, Luzón F, Navarro M, Santoyo MA (2010) Assesing the reliability of the single circular array method for love wave surveying. Bull Seismol Soc Am 100(5A):2230–2249

García-Mayordomo J (2005) Caracterización y Análisis de la Peligrosidad Sísmica en el Sureste de España. Tesis Doctoral. Universidad Complutense de Madrid, pp 373

García-Mayordomo J, Álvarez-Gómez JA (2006) Estimación del terremoto máximo posible y su intervalo de recurrencia en la Falla de Carrascoy (Murcia) para su implementación en el cálculo de la peligrosidad sísmica de la región. Geogaceta 39:51–54

García-Mayordomo J, Martínez-Díaz JJ (2006) Caracterización sísmica del Anticlinorio del Bajo Segura (Alicante): Fallas del Bajo Segura, Torrevieja y San Miguel de Salinas. Geogaceta 40:19–22

Instituto Andaluz de Geofísica (IAG) (2011) Terremoto Lorca (11 Mayo 2011), estudios preliminares, Granada. Available at http://www.ugr.es/_iag

Instituto Geográfica Nacional (IGN) (2011) Serie terremoto NE Lorca (Murcia), Madrid. Avaialble at http://www.ign.es

Instituto Geológico y Minero de España (IGME) (1992) Estudio de la peligrosidad y vulnerabilidad sísmica en Lorca y su término municipal. Ed.: IGME and Murcia Government, p 197

Ismet A, Tildy P, Prónay Z, Pinar A, Hermann L (2006) VS30 mapping and soil classification for seismic site effect evaluation in Dinar region, SW Turkey. Geophys J Int 165:223–235

Lachet C, Hatzfeld D, Bard PY, Theodulidis N, Papaioannou C, Savvaidis A (1996) Site effects and microzonation in the city of Thessaloniki (Greece) comparison of different approaches. Bull Seismol Soc Am 6:1692–1703

Laouamia N, Slimania A, Bouhadada Y, Chatelaina JL, Noura A (2006) Evidence for fault-related directionality and localized site effects from strong motion recordings of the 2003 Boumerdes (Algeria) earthquake: Consequences on damage distribution and the Algerian seismic code. Soil Dyn Earthq Eng 26(11):991–1003

Luzón F, Almendros J, García-Jerez A (2011) Shallow structure of deception Island, Antarctica, from correlations of ambient seismic noise on a set of dense seismic arrays. Geophys J Int 185:737–748

Maqsood ST, Schwarz J (2008) Analysis of building damage during the 8 October 2005 earthquake. Pak Seismol Res Lett 79:163–177

Martínez Díaz JJ, Hernández-Enrile JL (2001) Using travertine deformations to characterize paleoseismic activity on an active oblique-slip fault: the Alhama de Murcia Fault (Betic Cordillera-Spain). Acta Geol Hispanica Geol Acta 36(3–4):297–313

Masana E, Martínez-Díaz JJ, Hernández-Enrile JL, Santanach P (2004) The Alhama de Murcia fault (SE Spain), a seismogenic fault in a diffuse plate boundary: Seismotectonic implications for the Ibero-Magrebian region. J Geophys Res 109:B01301

Mayne PW, Rix GJ (1993) Relationships for clay. Geotech Test J 16:54–60

Mucciarelli M, Masi A, Gallipoli MR, Harabaglia P, Vona M, Ponzo F, Dolce M (2002) Analysis of RC building dynamic response and soil-building resonance based on data recorded during a damaging earthquake (Molise, Italy, 2002). Bull Seismol Soc Am 94(5):1943–1953

Nakamura Y (1989) A method for dynamic characteristics estimation of subsurface using microtremor on the ground surface. Q Rep Railw TechRes Inst 30:25–33

Navarro M, Corchete V, Badal JI, Pujades L, Canas JA, Vidal F (1997) Inversion of Rg waveforms in southern Spain. Bull Seismol Soc Am 87:847–865

Navarro M, Sánchez FJ, Enomoto T, Vidal F, Rubio S (2000) Relation between the predominant period of soil ant the damage distribution afther Mula 1999 earthquake. In: 6th international conference on seismic zonation (6ICSC). Palm Spring, California

Navarro M, Vidal F, Feriche M, Enomoto T, Sánchez FJ, Matsuda I (2004) Expected ground-RC building structures resonance phenomena in Granada city (southern Spain). In: 13th world conference on earthquake engineering. Vancouver, (paper 3308) p 11

Navarro M, Vidal F, Enomoto T, Alcalá FJ, Sánchez FJ, Abeki N (2007) Analysis of site effects weightiness on RC building seismic response. The Adra (SE Spain) example. Earthq Eng Struct Dyn 36:1363–1383

Navarro M, Enomoto T, Yamamoto T, García-Jerez A, Vidal F, Bretón M (2008) Analysis of site effects and their correlation with damage distribution observed during the Colima (Mexico) earthquake of January 21, 2003. In: Proceeding 14th world conference on earthquake engineering, Beijing

Nazarian S (1984) In situ determination of elastic moduli of soil deposits and pavement systems by spectral analysis of surface waves method. Ph.D. dissertation, University of Texas, Austin

NCSE-02 (2002) Normativa de Construcción Sismorresistente Española. Comisión Permanente de Normas Sismorresistentes, Real Decreto 997/2002. Boletín Oficial Del Estado No. 244

NEHRP (2003) Recommendation prevision for seismic regulation for new buildings and other structures, Building Seismic Saftey Council, Washington, Federal Emergency, FEMA

Ohta Y, Goto N (1978) Empirical shear wave velocity equations in terms of characteristic soil indexes. Earthq Eng Struct Dyn 6:87–167

Olsen KB, Archuleta RJ, Matarese JR (1995) Three-dimensional simulation of a magnitude 7.75 earthquake on the San Andreas fault. Science 270:1628–1632

Paquet J (1969) Étude géologique de l'Ouest de la province de Murcie (Espagne). Bull Soc Géol France 111:1–270

Parolai S, Picozzi M, Richwalski SM, Milkereit C (2005) Joint inversion of phase dispersion and H/V ratio curves from seismic noise recordings using a genetic algorithm. Geophys Res Lett 32:L01303

Park CB, Miller RD, Xia J (1999) Multichannel analysis of surface waves. Geophysics 64(3):800–808

Paterson MS (1978) Experimental rock deformation—the brittle field. Springer, New York, p 254

Peng Cui, Xiao-Qing Chen, Ying-Yan Zhu, Feng-Huan Su, Fang-Qiang Wei, Yong-Shun Han, Hong-Jiang Liu, Jian-Qi Zhuang (2011) The Wenchuan earthquake (May 12, 2008), Sichuan Province, China, and resulting geohazards. Nat Haz 56(1):19–36

Sanz de Galdeano C, Lopez Casado C, Delgado J, Peinado MA (1995) Shallow seismicity and active faults in the Betic Cordillera. A preliminary approach to seismic sources associated with specific faults. Tectonophysics 248:293–302

SESAME (2004) Guidelines for the implementation of the H/V spectral ratio technique on ambient vibrations. Measurements, processing and interpretation. SESAME European research project WP12-deliverable D23.12. http://sesame-fp5.obs.ujf-grenoble.fr/Delivrables/Del-D23-HV_User_Guidelines.pdf

Silva PG, Goy L, Zazo C (1992) Características estructurales y geométricas de la falla de desgarre de Lorca-Alhama. Geogaceta 12:8–9

Sykora DW, Koester PJ (1988) Correlations between dynamic shear resistance and standard penetration resistance in soils. Earthq Eng Soil Dyn 2:389–404

Tokimatsu K (1997) Geotechnical site characterization using surface waves. In: Ishihara K (ed) Earthquake geotechnical engineering. Balkema, Rotterdam, pp 1333–1368

Towhaka I, Roteix R (1988) Probabilistic estimation of shear wave velocity of sands in terms of SPT-N and its application to seismic response analysis. In: Proceedings of the annual meeting of Japanese soil mechanics and foundation engineering, pp 825–828

Vidal F (1986) Sismotectónica de la región Béticas-Mar de Alborán. Tesis Doctoral. Universidad de Granada

Vidal F, Mourabit T, Navarro M, Enomoto T, Feriche M (2004) A preliminary account of the intensity and structural damage of the 24 february 2004 Al Hoceima (Morocco) earthquake. XXIX General Assembly of the European Seismological Commission, Postdam

Vidal F, Navarro M, Aranda C, Enomoto T (2012) Fundamental period and damping shift due to 2011 Lorca (Spain) earthquake from in-situ ambient noise measurements. Bull Earthquake Eng. (In this issue)

Wang Z (2001) Fundamentals of seismic rock physics. Geophysics 66:398–412

Zeck HP, Albat F, Hansen BT, Torres-Rodán RL, García-Casco A, Martín-Algarra A (1989) A 21 ± 2 Ma age for the termination of the ductile Alpine deformation in the internal zone of the Betic Cordilleras, South Spain. Tectonophysics 169:215–220